AEDC-TR-76-61

cy.5

AN INVESTIGATION OF THE USE OF THE FABRY-PEROT INTERFEROMETER FOR FLOW FIELD DIAGNOSTICS USING RAMAN SCATTERING

VON KÁRMÁN GAS DYNAMICS FACILITY
ARNOLD ENGINEERING DEVELOPMENT CENTER
AIR FORCE SYSTEMS COMMAND
ARNOLD AIR FORCE STATION, TENNESSEE 37389

June 1976

Final Report for Period July 1, 1974 — July 21, 1975

Approved for public release; distribution unlimited.

Prepared for

DIRECTORATE OF TECHNOLOGY (DY)
ARNOLD ENGINEERING DEVELOPMENT CENTER
ARNOLD AIR FORCE STATION, TENNESSEE 37389

NOTICES

When U. S. Government drawings specifications, or other data are used for any purpose other than a definitely related Government procurement operation, the Government thereby incurs no responsibility nor any obligation whatsoever, and the fact that the Government may have formulated, furnished, or in any way supplied the said drawings, specifications, or other data, is not to be regarded by implication or otherwise, or in any manner licensing the holder or any other person or corporation, or conveying any rights or permission to manufacture, use, or sell any patented invention that may in any way be related thereto.

Qualified users may obtain copies of this report from the Defense Documentation Center.

References to named commercial products in this report are not to be considered in any sense as an endorsement of the product by the United States Air Force or the Government.

This report has been reviewed by the Information Office (OI) and is releasable to the National Technical Information Service (NTIS). At NTIS, it will be available to the general public, including foreign nations.

APPROVAL STATEMENT

This technical report has been reviewed and is approved for publication.

FOR THE COMMANDER

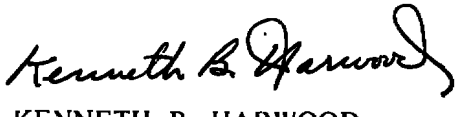

KENNETH B. HARWOOD
Major, CF
Research & Development
Division
Directorate of Technology

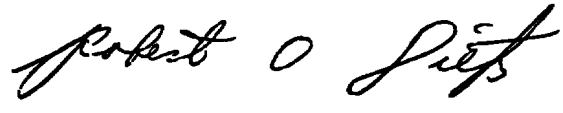

ROBERT O. DIETZ
Director of Technology

REPORT DOCUMENTATION PAGE		READ INSTRUCTIONS BEFORE COMPLETING FORM
1 REPORT NUMBER AEDC-TR-76-61	2 GOVT ACCESSION NO.	3 RECIPIENT'S CATALOG NUMBER
4 TITLE (and Subtitle) AN INVESTIGATION OF THE USE OF THE FABRY-PEROT INTERFEROMETER FOR FLOW FIELD DIAGNOSTICS USING RAMAN SCATTERING		5 TYPE OF REPORT & PERIOD COVERED Final Report - July 1, 1974 - July 21, 1975 6 PERFORMING ORG REPORT NUMBER
7 AUTHOR(s) D. P. Weaver and J. W. L. Lewis ARO, Inc.		8 CONTRACT OR GRANT NUMBER(s)
9 PERFORMING ORGANIZATION NAME AND ADDRESS Arnold Engineering Development Center (DY) Air Force Systems Command Arnold Air Force Station, Tennessee 37389		10 PROGRAM ELEMENT, PROJECT, TASK AREA & WORK UNIT NUMBERS Program Element 65807F
11 CONTROLLING OFFICE NAME AND ADDRESS Arnold Engineering Development Center (DYFS) Air Force Systems Command Arnold Air Force Station, Tennessee 37389		12 REPORT DATE June 1976 13 NUMBER OF PAGES 38
14 MONITORING AGENCY NAME & ADDRESS(if different from Controlling Office)		15 SECURITY CLASS. (of this report) UNCLASSIFIED 15a DECLASSIFICATION/DOWNGRADING SCHEDULE N/A

16 DISTRIBUTION STATEMENT (of this Report)

Approved for public release; distribution unlimited.

17 DISTRIBUTION STATEMENT (of the abstract entered in Block 20, if different from Report)

18 SUPPLEMENTARY NOTES

Available in DDC

19 KEY WORDS (Continue on reverse side if necessary and identify by block number)

Raman scattering
rotational temperature
number density
measurement
gases
interferometer

20 ABSTRACT (Continue on reverse side if necessary and identify by block number)

A new interferometric technique for the detection of rotational Raman scattering was demonstrated. The technique involves the use of a Fabry-Perot interferometer to simultaneously pass all of the rotational lines from a single molecular specie while at the same time rejecting interfering light from other molecular species and that of Rayleigh scattered light. Data were obtained for total ground state rotational Raman scattering intensity versus interferometer plate separation. Measurements for total rotational Raman

DD FORM 1 JAN 73 1473 EDITION OF 1 NOV 65 IS OBSOLETE

20. ABSTRACT (Continued)

signal versus gas pressure were also obtained which demonstrated a gain in sensitivity over conventional detection techniques. In addition, the capability of the interferometer to reject interfering rotational spectra from other gas species is demonstrated. Calculations are presented which predict the rotational temperature dependence of the transmitted intensity of the Fabry-Perot interferometer. The use of the technique for both rotational and vibrational temperature measurements as well as determination of molecular number density is discussed. The results of this study indicate that a significant increase in sensitivity for a Raman scattering measurement of both density and temperature can be obtained using Fabry-Perot interferometry. Additionally, it was found that, for a wide temperature range, the N_2 density measurement can potentially be made without knowledge of the gas temperature.

AFSC
Arnold AFS Tenn

PREFACE

The work reported herein was conducted by the Arnold Engineering Development Center (AEDC), Air Force Systems Command (AFSC), under Program Element 65807F. The results were obtained by ARO, Inc. (a subsidiary of Sverdrup & Parcel and Associates, Inc.), contract operator of AEDC, AFSC, Arnold Air Force Station, Tennessee. The work was done under ARO Project Nos. V32S-37A and V32S-06A. The authors of this report were D. P. Weaver and J. W. L. Lewis, ARO, Inc. The manuscript (ARO Control No. ARO-VKF-TR-75-129) was submitted for publication on August 13, 1975.

CONTENTS

ILLUSTRATIONS

TABLES

1.0 INTRODUCTION AND THEORY

1.1 FLOW DIAGNOSTICS USING A FABRY-PEROT INTERFEROMETER

The measurement of both rotational temperature and number density using laser Raman scattering has been successfully accomplished in high-speed flow fields of aerospace test facilities (Refs. 1 and 2). Two anticipated difficulties in the application of the technique are, first, the need for high spectral resolution for rotational Raman scattering (RRS) from a gas mixture, the species having comparable rotational constants; and second, the low signal level of the scattering process. Both of these difficulties are ameliorated in principle with the replacement of the usually employed dispersive spectrometer by a Fabry-Perot interferometer (FPI). The high resolution of the FPI is well known and needs no elaboration. The increase in RRS signal level is a result of both a gain in luminosity and operation of the FPI as a Dirac comb filter (Refs. 3 through 5) where the transmission maxima of the FPI are made coincident with the periodic RRS spectrum. The increase in luminosity relative to the dispersive spectrometer can be shown to be $4\pi/\beta$ where β is the angle subtended by the spectrometer slit at the source. Obviously, if β is at its maximum value of 2π, the luminosity gain is two. For typical conditions, β is on the order of 0.02 to 0.10 radians, which results in a luminosity gain on the order of 100.

The gain in signal level for RRS, as a result of using the FPI as a comb filter, can most easily be seen by recognizing that all RRS spectral lines are transmitted simultaneously and are manifested as a focused FPI ring pattern. Consequently, for detection of the RRS photons, one reaps the advantage of multiplexing which is approximately one order of magnitude gain in sensitivity, and the data acquisition time is reduced accordingly.

Further, it is suggested that rotational temperature (T_R) measurements, in addition to specie density (n), are possible by spectrally blocking the RRS anti-Stokes radiation and passing only the RRS Stokes signal. This signal, when ratioed to the total RRS-FPI output signal with no spectral blocking will provide a unique value of T_R.

Consequently, the use of the FPI offers distinct advantages for flow field diagnostics using Raman scattering, and this report describes the initial investigation of the use of the FPI for this application.

1.2 THEORY OF THE FABRY-PEROT INTERFEROMETER

The Fabry-Perot interferometer consists of two optically flat quartz plates which produce interference fringes as a result of multiple reflections from the partially transparent inner surfaces of each plate. The intensity (I_t) of radiation transmitted by the FPI for an incident intensity (I_o) of wavelength (λ) is given by the well-known Airy function (Ref. 6):

$$I_t/I_o = [1 - (\frac{A}{1-R})]^2 [1 + F \sin^2 (\delta/2)]^{-1} \quad (1)$$

where A and R are the absorptance and reflectance of the plates of the FPI. The transmittance T is given by

$$T + R + A = 1$$

and the quantity F is defined as $4R/(1 - R)^2$. The angular function δ is given by

$$\delta = (4\pi/\lambda) \times \mu \times d \times \phi' - 2\Phi \quad (2)$$

where μ is the index of refraction of the medium between the interferometer plates of separation distance (d), ϕ' is the angle of refraction within the first plate, and Φ is a general phase angle for the reflection process. Obviously for a lossless system, normal incidence of radiation, and for $\Phi = \pi$,

$$\delta = (4\pi\mu d/\lambda) + 2\pi \quad (3)$$

Defining the order of interference (m) to be $\delta/2\pi$ gives

$$m = (2\mu d/\lambda) + 1$$

From Eq. (1), it is seen that transmission maxima occur periodically when δ equals $2\pi m$ and occur with an angular frequency (ω) interval

$$\Delta\omega = 1/(2\mu d) \quad (4)$$

$\Delta\omega$ is the free spectral range of the FPI.

For monochromatic incident light of angular frequency (ω), expressed in wavenumbers, then it is seen from Eq. (4) that maxima of I_t will occur for mirror displacements Δd equal to

$$\Delta d = 1/2\mu\omega = \lambda/2\mu \quad (5)$$

or for half wavelength displacements of the mirrors. Thus, by varying d, the free spectral range may be adjusted to be equal to the frequency spacing of lines occurring in periodic spectra such as those found in a pure rotational Raman spectrum. Used in this manner, the interferometer is essentially a comb filter in which the teeth of the comb exactly match a given periodic spectrum and thus transmit all of the lines in the spectrum simultaneously.

The use of this technique for the detection of a given rotational Raman spectrum is illustrated in Fig. 1, and the effects of molecular centrifugal distortion have been neglected. The frequency distribution of spectral lines for a pure rotational Raman spectrum is given by (Ref. 7):

$$\omega_J = \omega_o \pm 4B(J + 3/2) \qquad (6)$$

where ω_o is the frequency of the exciting laser source, B is the rotational constant (in wave numbers) for the particular specie under consideration, and J is the rotational quantum number. Figure 1a is a schematic representation of a spectrum predicted by Eq. (6). The first two rotational

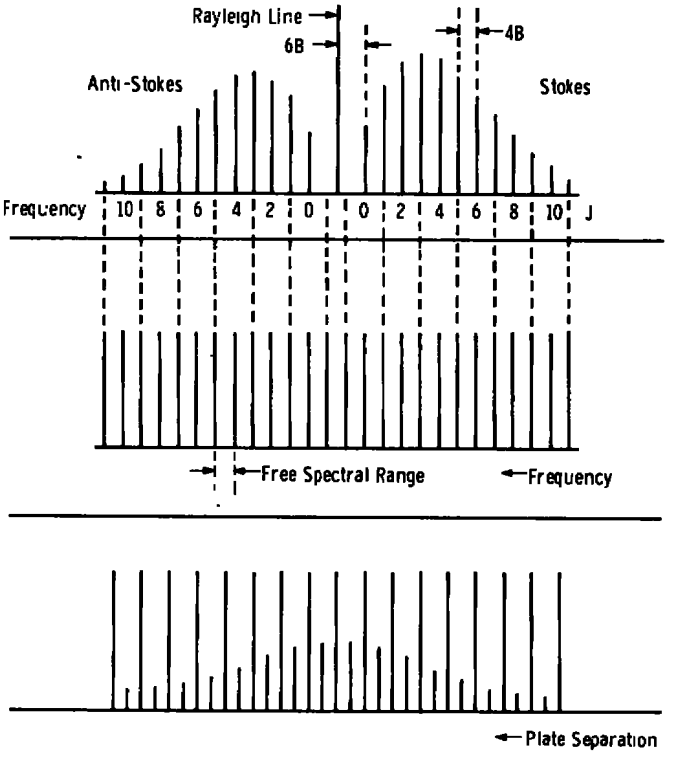

a. Pure rotational Raman spectrum for N_2

b. Transmission profile for a Fabry-Perot interferometer

c. Interferogram profile resulting from scanning the FPI

Figure 1. Schematic representation of the interferogram profile.

Raman lines (J = 0) are shifted away from the exciting frequency by a value equal to 6B, whereas the frequency of separation between the individual rotation lines is found to be 4B. In Fig. 1b, the vertical lines represent the transmission peaks of the Fabry-Perot interferometer for a free spectral range of 4B. For this case, there is a one-to-one correspondence between the transmission peaks of the Fabry-Perot and the rotational Raman lines from the specie under investigation. As can be seen, all of the rotational Raman lines will be transmitted as a single interference fringe maxima, and the Rayleigh scattered light will be blocked. As the interferometer plate separation (d) is scanned by a value equal to $1/(4\mu\omega_o)$, the Rayleigh line will be transmitted, and all of the rotational Raman lines will be blocked. For $\omega_o \simeq 20,000$ cm^{-1}, alternation of transmission of first Rayleigh and then Raman lines occurs as d is varied by 1,250 Å. The resulting interferogram, obtained by varying the interferometer plate separation in the region about $d = 1/(8\mu B)$, is represented in Fig. 1c. The vertical lines of constant amplitude represent the Rayleigh fringes, and the smaller vertical lines of varying amplitude represent the Raman fringes. The Raman fringe has a maximum value when the teeth of the transmission comb best match the rotational Raman spectrum. Clearly, for different species and, consequently, different values for the rotational constant B, the Raman fringe maxima are observed for plate separations $d = 1/(8\mu B)$.

Centrifugal distortion of the molecule produces a small J-dependent variation of the frequencies (ω_J) of the rotational Raman lines. The only result of the inclusion of this effect is that the case of a perfect coincidence of all of the rotational Raman lines with the Fabry-Perot comb can never be exactly realized, and this will result in a slight decrease in the amplitude of the interferogram maxima.

It is possible to obtain other interference patterns for values of the free spectral range equal to certain multiples of the rotational gas constant. These other cases can be advantageously used to reject unwanted light from other species present in the sample region. However, for the scope of this report, only the 4B resonance case for N_2 is of interest. A more complete discussion of these other effects can be found in Refs. 3 through 5, 8, and 9 and will not be discussed at this time.

2.0 EXPERIMENTAL APPARATUS

The experimental apparatus used to study the rotational Raman spectra of nitrogen is shown in Fig. 2. The exciting source was a

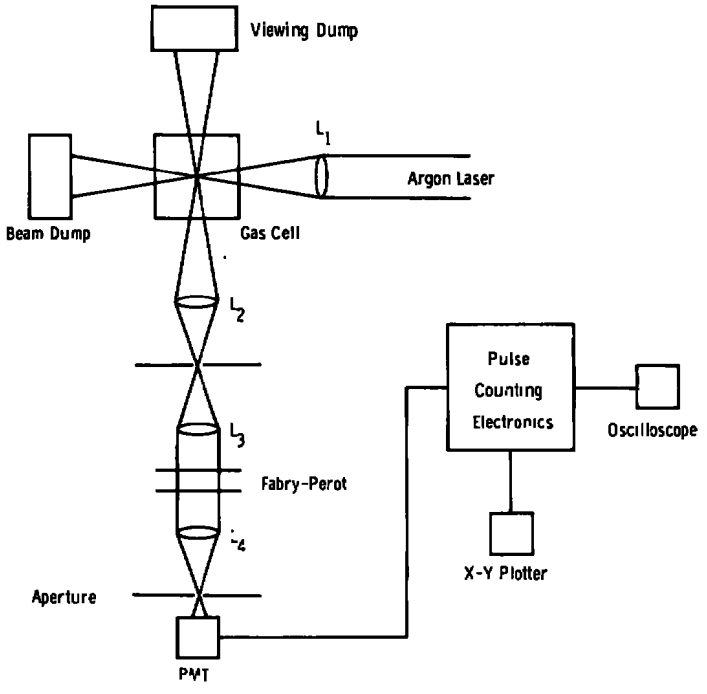

Figure 2. Schematic of the laboratory experimental arrangement.

Coherent Radiation Model CR-5 argon-ion laser manually operated at a nominal power level of 3.5 W at either 488.0 or 514.5 nm wavelength. As shown in Fig. 2, the unexpanded laser beam was focused by a 50.8-mm-diam fused-silica lens of 250-mm focal length into the center of the gas scattering chamber. Using the relations of Schwiesow (Ref. 10) the diameter of the observed scattering volume was calculated to be 220.5 μm. The scattering cell was the same as that used by Williams and Lewis (Ref. 11) and was made of black anodized aluminum. The laser beam entered the scattering chamber through a fused-silica window, and from the focal point at the center of the chamber, the beam expanded and entered a specially prepared laser dump. The dump consisted of a 72-cm-long, 5-deg offset cone of black anodized aluminum. The cone was located within a closed end piece of black anodized aluminum tubing which was bolted to the scattering cell. The focal region of the laser beam was observed at 90 deg through a fused-silica window. Directly across the cell from the observation port was a viewing dump that consisted of a black anodized 15-deg cone of 25.4-cm length housed in a closed end piece of black anodized aluminum tubing which was bolted to the scattering cell. The viewing dump provided a background for the observation of the focal region of the laser beam.

The entire scattering chamber could be evacuated to a pressure of 10^{-5} torr and was essentially leak-free. Nitrogen was leaked into the chamber through a series of valves, including a needle valve, which were connected to a high-pressure gas bottle. Pressure in the chamber was measured with calibrated Wallace and Tiernan-, Texas Instruments Quartz-, and MKS Baratron-pressure gages.

The scattered radiation was collected by a 7.62-cm-diam, 12.7-cm focal length glass collection lens. The collected light was focused onto the surface of a circular aperture located approximately 20 cm from the collection lens. A magnification of 0.60 was thus obtained. By adjusting the size of the aperture, any length of beam could be observed. For this study, a 1-mm length of laser beam was observed. The collected light that passed through the aperture was then collimated by a 50.8-mm-diam, 250-mm focal length, fused-silica lens which was located 250-mm from the limiting aperture. The collimated light then passed through a second aperture which was mounted on the front of the Fabry-Perot interferometer. This aperture proved to be the limiting aperture in the collection optics system and was set to a diameter of 0.60 mm. The resulting collection solid angle was 2.97×10^{-3} sr. The collimated light then passed through the Fabry-Perot interferometer.

The Fabry-Perot interferometer consists of two Burleigh Instruments fused-quartz, 37.5-mm, $\lambda/100$ interferometer flats mounted between an invar spacer. The plates are slightly prismatic to avoid unwanted effects of reflections at the outer uncoated surfaces. The flats were coated for a a reflectance of R = 97.5 percent in the region 488.0 to 550.0 nm (see Fig. 3). The interferometer plate separation was set at approximately 0.0625 cm for this experiment, which yields a free spectral range of 8.000 cm^{-1}. The overall working finesse of the system, which is defined as the ratio of the free spectral range to the full width at half maximum of the Rayleigh peak, was between 20 and 30, which, for the plate separation used, corresponds to a resolution from 0.40 to 0.27 cm^{-1}. This approaches the maximum finesse obtainable with the argon laser of 0.15 cm^{-1} line width.

The interferometer was used in two modes. In the scanning mode, the spectral content of the incident light was observed by moving one mirror along the interferometer axis without disturbing the parallelism of the mirrors. This was accomplished through the combined use of a differential screw assembly for coarse motion and three Burleigh Instruments PZT-4 piezoelectric transducer (PZT) stacks for fine tuning. The differential screw and transducer stacks were attached to one mirror;

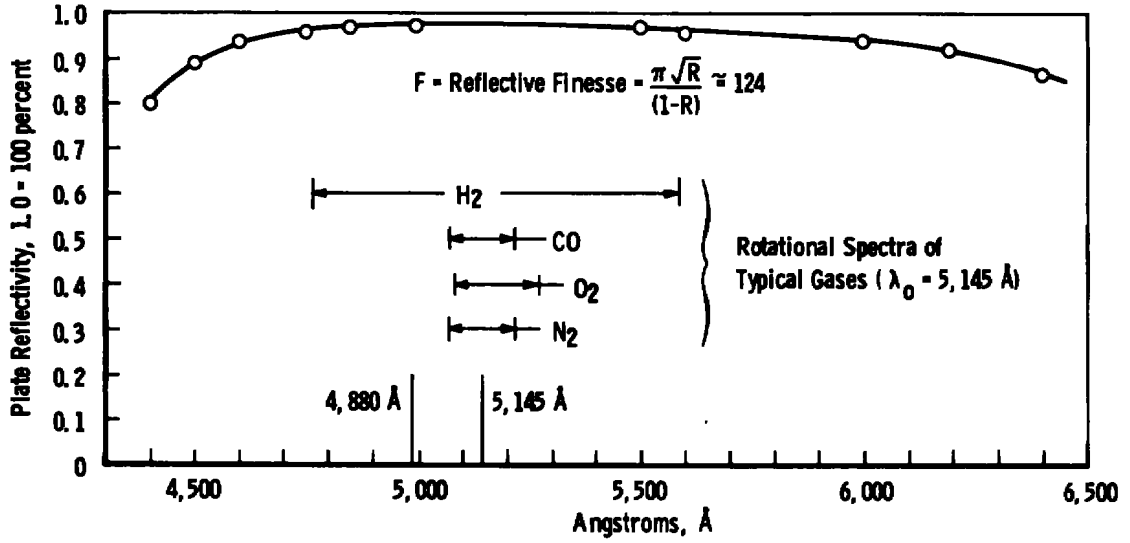

Figure 3. Mirror reflectivity versus wavelength for the FPI.

the second mirror was stationary. After an initial and coarse alignment, the PZT stacks were used for fine tuning and for scanning. The PZT transducers expand at a rate of 17 Å/V when a voltage is applied along the poling direction of the ceramic. A ramp voltage was applied in the scanning mode by a Burleigh Instruments Model RC-41 generator. In the static or filter mode, the mirrors remain stationary and transmit a selected wavelength. Selection of desired wavelength is accomplished by using the PZT transducers with a variable d-c voltage. After passing through the interferometer, the collimated light was focused by a 50.8-mm fused-silica focusing lens of 250-mm focal length onto the surface of an aperture which was mounted on the front of the photomultiplier tube housing. The focused light passed through the aperture and expanded onto the photocathode surface of the photomultiplier.

In order to record photoelectrically the interference fringes, the Fabry-Perot fringe pattern (see Fig. 4) is imaged onto a focal plane containing a small circular hole at the center of the fringe pattern. For this experiment, a 1.5-mm-diam aperture was used. This aperture allows only the light from the center fringe to be transmitted to the photomultiplier. The interferometer is scanned by piezoelectrically changing the optical path between the interferometer mirrors. If, for example, the interferometer is scanned by varying d by one-half wavelength, the center fringe will disappear, and the first ring will collapse to form the center fringe. If the bright center fringe of Fig. 4 corresponds to the nth interference order at 488.0 nm, then the first interference ring is the $(n + 1)^{th}$ order at 514.5 nm. The central fringe could, however, be formed by the $(n + 1)^{th}$ order for a wavelength slightly different than

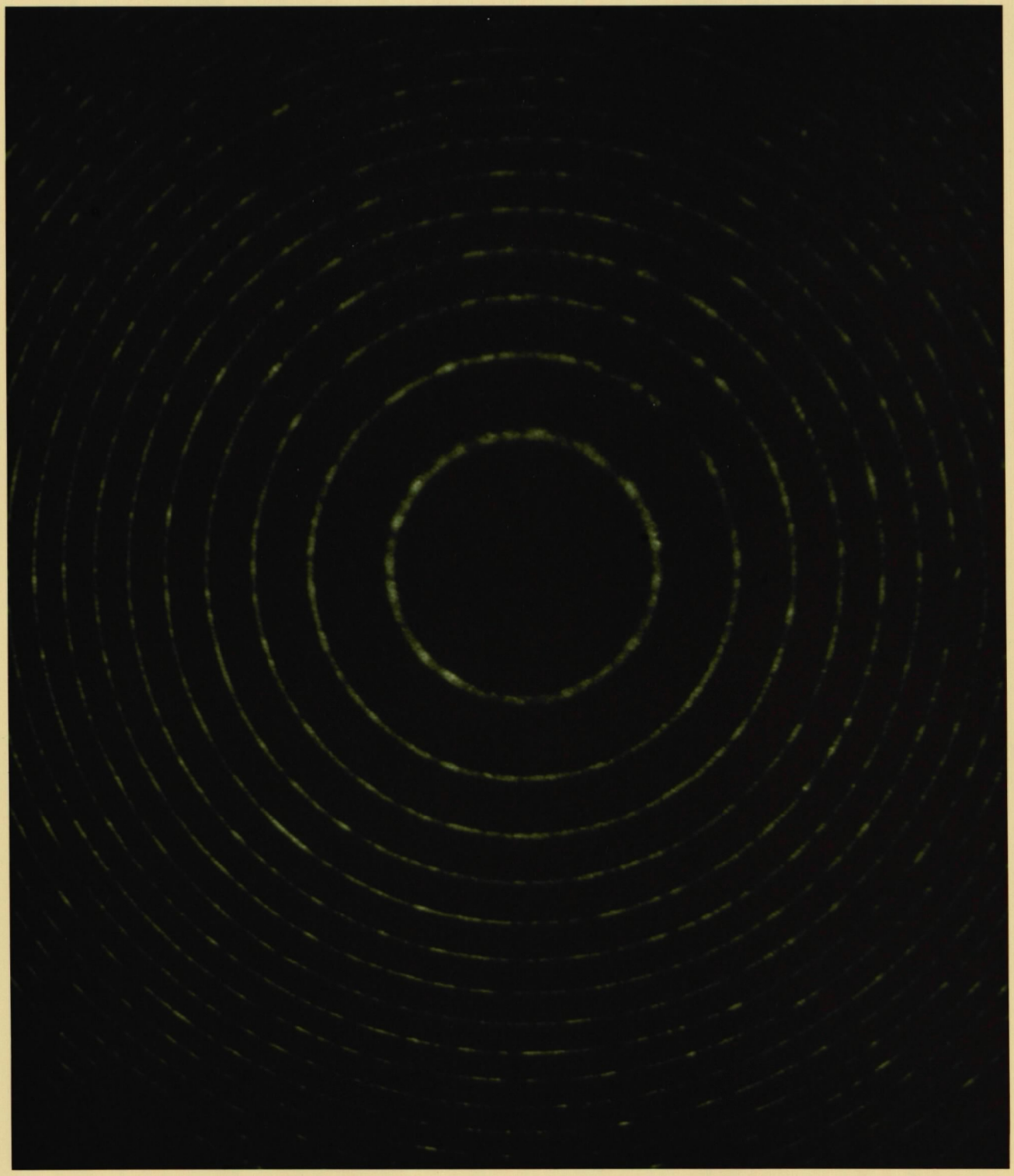

Figure 4. Photograph of the Fabry-Perot interference fringes for 5145 Å illumination from an argon-ion laser.

488.0 nm. Clearly, any wavelength of radiation differing from ω_o by integral multiples of the free spectral range will produce the center fringe. This is the filtering property of the Fabry-Perot interferometer which is used advantageously to transmit simultaneously all the rotational Raman lines from a gas.

The photomultiplier tube was an EMI-9502B with a 10-mm-diam photocathode. The tube was contained in a thermoelectrically cooled, Products for Research, Inc., Model TE-104 housing. The housing could operate continuously at -26°C, which provided a reduction in dark current by approximately a factor of 45 from the room temperature value. Power to the photomultiplier was supplied by a Precision Power Supply Model 122B.

The output of the photomultiplier tube was processed by an ORTEC photon counting system which is shown in block diagram form in Fig. 5.

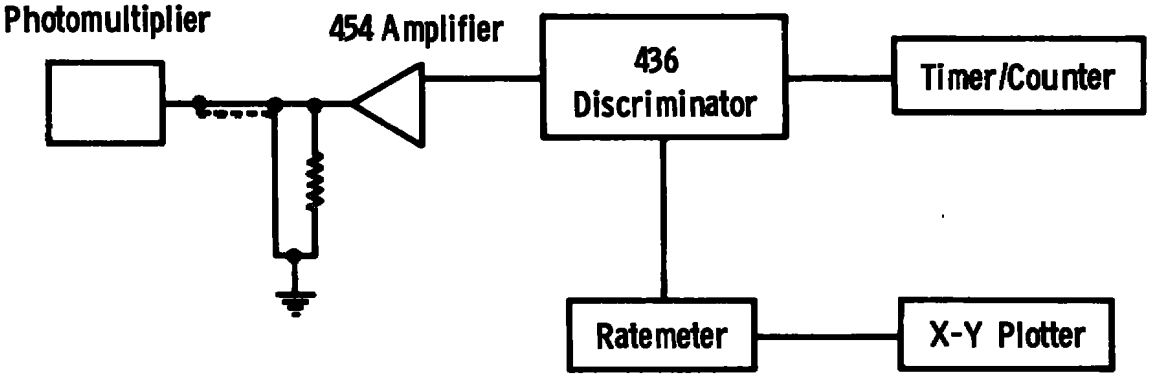

Figure 5. Block diagram of the photon counting system.

The coaxial output cable from the photomultiplier tube was terminated with a 50-ohm resistor at the Model 454 amplifier input. The amplifier pulses were then passed through a Model 436 discriminator to both a Model 715 dual counter/timer and a Model 441 ratemeter. The ratemeter output was displayed by either a Tektronix Model 502 oscilloscope or a Moseley Model 2DR-2A X-Y recorder.

3.0 RESULTS

3.1 INTERFEROGRAM MEASUREMENTS

Prior to each laboratory measurement, a careful optical alignment of the laser beam, scattering volume, collection optics, Fabry-Perot,

and detecting phototube had to be accomplished. With the argon laser operating at a very low power, the laser beam was aligned through the centerline of the gas scattering chamber. The quartz focusing lens was then inserted in the path of the laser beam 254 mm from the center of the cell and was autocollimated; i.e., aligned so that all reflecting beams from the lens pass back along the laser beam path. Next, with the gas scattering cell and quartz lens removed, a pentaprism was inserted at the position of the scattering volume. The pentaprism has the property of precisely deflecting an incident beam at 90 deg. By using this deflected beam which defined the collection optical axis, the Fabry-Perot interferometer was then aligned. In the static mode, the interferometer mirrors were set to a separation distance of 0.0625 mm using a feeler gage and the differential screws. The mirrors were then centered on the optical axis and autocollimated so that they were parallel to each other and perpendicular to the optical axis. Final adjustment was accomplished later piezoelectrically. The phototube was then placed on the optical axis so that the beam of laser light passed through the center of the photomultiplier tube housing aperture and illuminated the center of the photocathode surface. Finally, the collection, collimation, and focusing lenses were placed on the optical axis and autocollimated; the pentaprism was removed, and the gas scattering cell and focusing lens were replaced. Final adjustment of the collection optics system was then made by filling the gas cell with pipe smoke and observing the image of the scattering volume on the selecting aperture and the pinhole aperture at the photomultiplier. By very small adjustments of the collection lens, the central fringe diameter was centered on the pinhole aperture. The aperture diameter was then made equal to the central fringe diameter.

After evacuating the gas chamber to 10^{-5} torr, nitrogen gas was slowly bled into the chamber until a pressure of one atmosphere was obtained. The Fabry-Perot interferometer was then set in the scanning mode so that the plate separation (d) was repetitively changed using the ramp generator and a scan rate of 5 FSR/sec. The output of the photomultiplier, or the transmission of the interferometer, was then displayed on the oscilloscope screen as a linear function of the mirror separation (Fig. 6). Final adjustment was made by observing the Rayleigh waveforms and using the PZT transducers to adjust for a maximum finesse.

Figure 7 shows the $\Delta\omega = 4B$ interferogram profile for rotational Raman scattering in N_2 gas at a pressure of one atmosphere and T_o equal to 295 K. This interferogram was generated by displacing one of the Fabry-Perot mirrors through a total distance of approximately 0.04 mm. This corresponds to a scan of about 175 orders at 488.0 nm. The large peaks

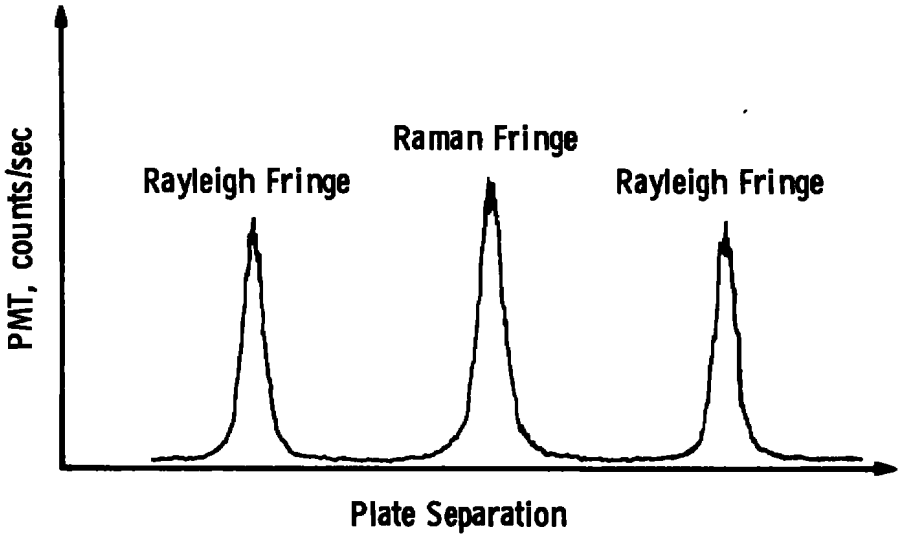

Figure 6. Transmitted intensity as a function of plate separation.

which are off scale in Fig. 7 are N_2 Rayleigh scattering peaks. Alternating with the Rayleigh fringes are the rotational Raman fringes. For the scans shown in Fig. 7, the ramp generator was set so that the plate separation was varied by one FSR in 100 sec for each average cavity separation (d), and as shown in Fig. 7, sixteen gross cavity steps, each of approximately 0.00125 mm, were made.

From Fig. 7, it is seen that, near 4B resonance, i.e., d = 1/(8B), both the Stokes and anti-Stokes components of the Raman spectrum contribute to the interferogram profile that has a single maximum. As the Fabry-Perot interferometer is scanned to greater (or smaller) plate separations, further from the resonance matching condition, however, the single maximum splits into two distinct maxima; one maximum corresponds to the Stokes component of the Raman spectrum, and the other to the anti-Stokes component. Eventually, when the plates have been scanned sufficiently far from the 4B resonance condition, no matches between the rotational Raman lines and the interferometer transmission comb occur, and the Raman signal is completely rejected.

The shape of the interferogram profile (or equivalently the number of single maxima observed) is a strong function of the rotational constant B of the particular gas under investigation. This may be demonstrated by considering N_2 which has a rotational constant B = 2.00065 cm^{-1} (Ref. 7) and HF which has a constant B = 20.5596 cm^{-1} (Ref. 7). To scan one free spectral range for either of the two molecules, the plate spacing must change by the same amount, i.e., $\lambda_o/2$ = 244.0 μm. The variation

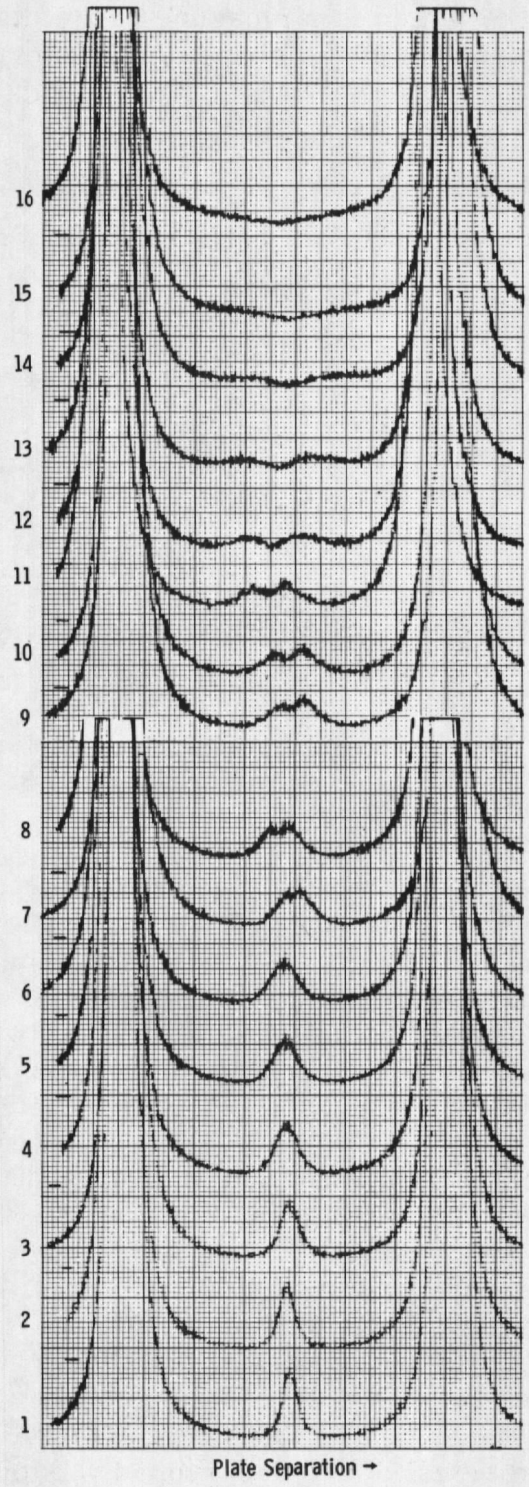

Figure 7. 4B resonance interferogram for N_2 with P_o = 1 atm and T_o = 295 K at plate separations d_1 to d_{16}.

in free spectral range, which is a measure of the matching condition and consequently representative of the shape of the interferogram profile, is found from Eq. (4) to be

$$\delta(\Delta\omega) = (2\mu d^2)^{-1} \tag{7}$$

For the 4B resonance condition $d = 1/(8\mu B)$, so that

$$\delta(\Delta\omega) = 32\mu B^2 \tag{8}$$

For the values of B given above,

$$\delta(\Delta\omega)_{N_2} = 128.08\ (cm^{-1})^2$$

and

$$\delta(\Delta\omega)_{HF} = 13526.31\ (cm^{-1})^2$$

for $\mu = 1$. Thus, the rate of change of the free spectral range $\Delta\omega$ with respect to d is about two orders of magnitude greater near the 4B resonance region for HF than for N_2. In both cases, however, the plate spacing is changed by the same amount so that the resonance condition for N_2 covers a much larger range of plate separations than does the resonance condition for HF.

3.2 NITROGEN DENSITY MEASUREMENTS

Nitrogen number density (n) measurements were performed with the same experimental arrangement used for the interferogram study. However, instead of scanning the plates over a wide range of d, the plate separation used was that corresponding to the nitrogen 4B resonance maximum; i.e., $d = 1/8\mu B = 0.0625$ cm where $B = 2.00065\ cm^{-1}$ for N_2.

The experimental system's alignment was checked using the method described previously. The scattering cell was then evacuated to 10^{-5} torr, and N_2 was slowly bled into the chamber until the desired pressure was obtained. The laser power was then set to 2.9 W at $\lambda_o = 488.0$ nm, and the interferometer was set to scan one FSR in 200 sec. The output of the photomultiplier was processed by the ORTEC counting system, and the variation in transmitted signal as obtained from the ratemeter versus plate separation was recorded by the Model 2DR-2A X-Y plotter (see Fig. 8). The Raman signal above background was obtained in this manner for a range of pressures. The results are shown in Fig. 9.

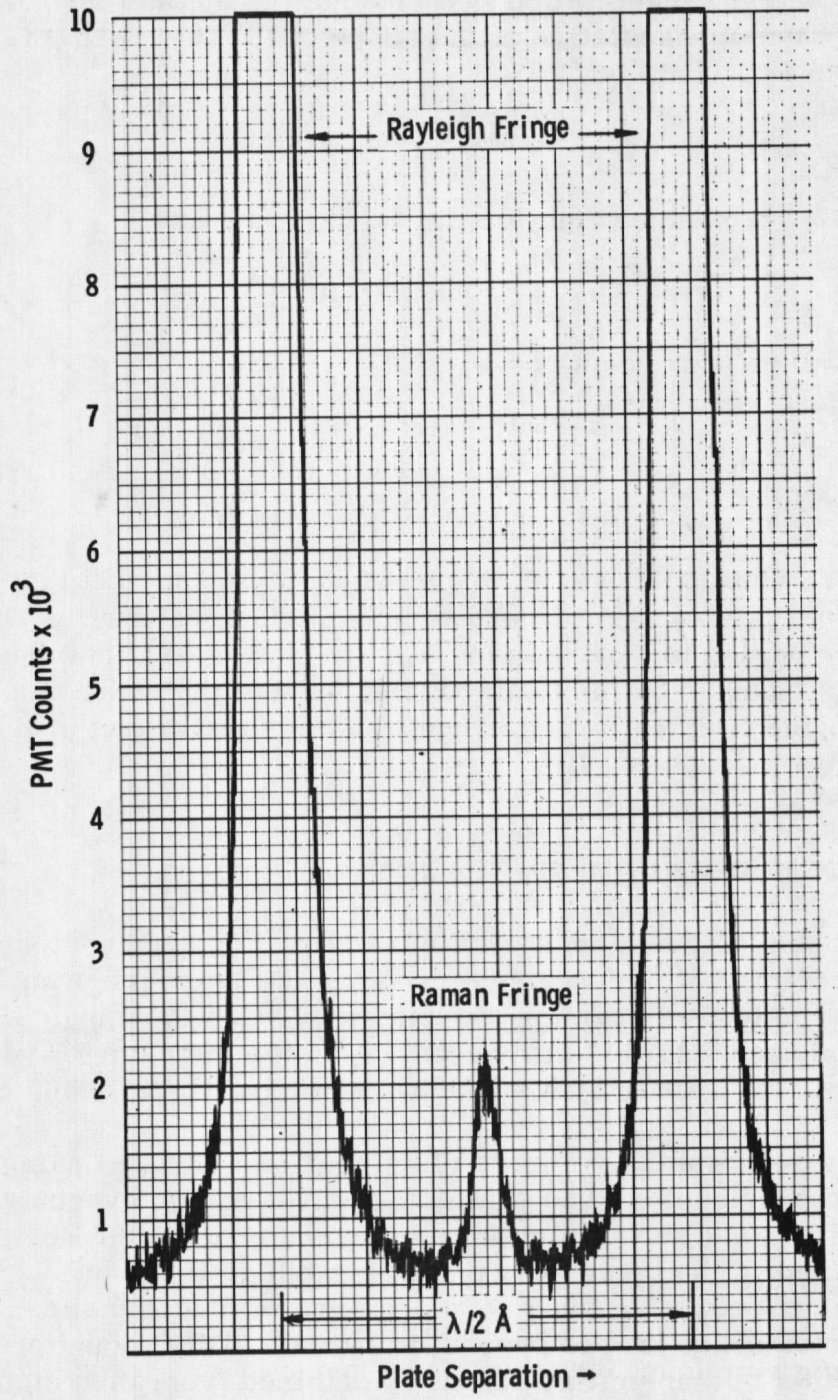

Figure 8. Pure rotational Raman spectrum for N_2: transmitted pattern with the FPI set to pass only N_2 rotational Raman lines.

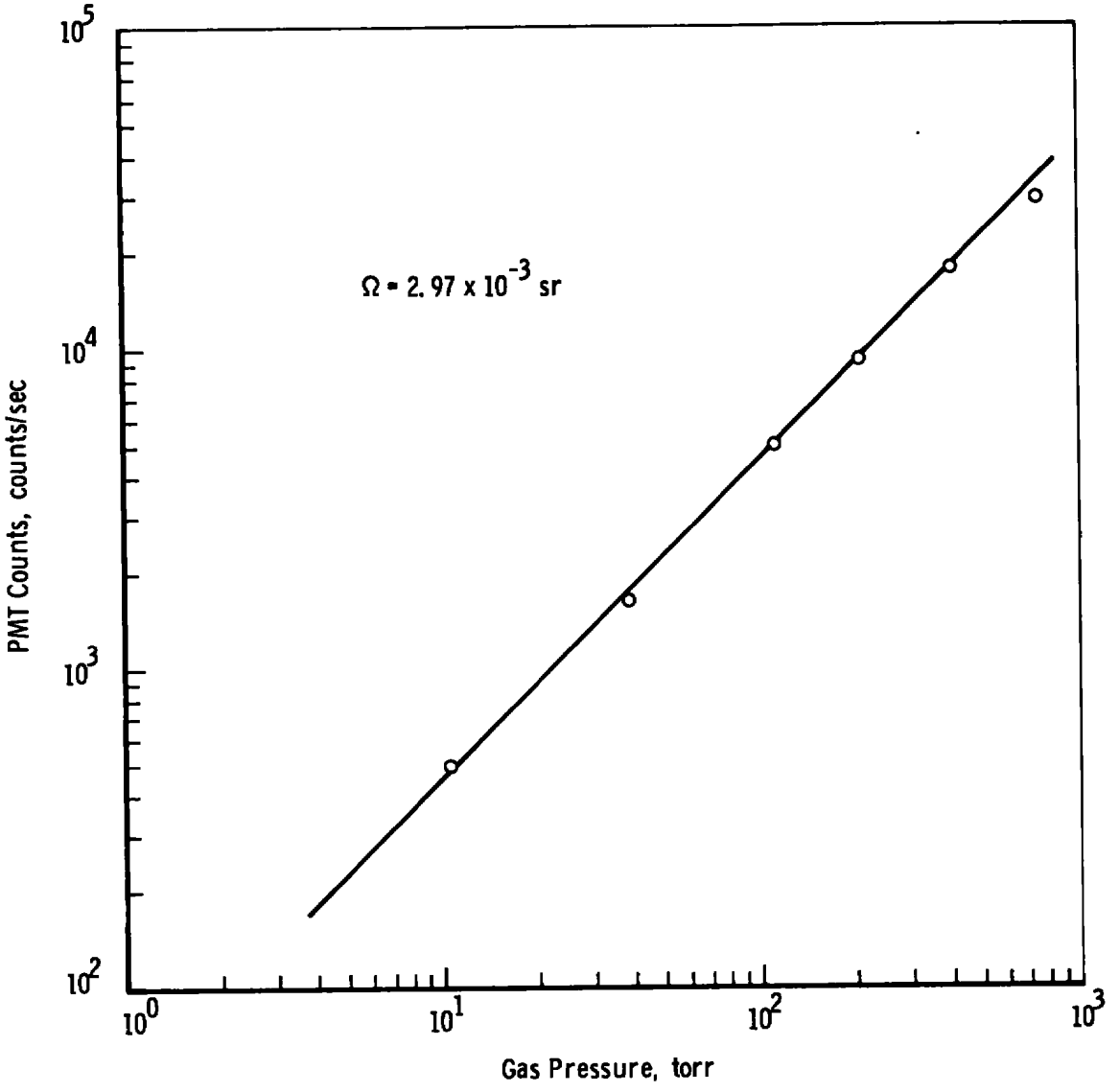

Figure 9. Variation of total pure rotational Raman signal with pressure for N_2 gas.

3.3 REJECTION OF SIGNAL FROM INTERFERING SPECIES

In order to investigate the ability of the Fabry-Perot to reject the interfering rotational Raman signal from impurity species, a similar procedure to that described in Section 3.2 was used. For this measurement, the plate separation was kept at the same value necessary for the nitrogen 4B resonance. The scattering cell was then evacuated to 10^{-5} torr, and CO_2 gas was in-bled to a pressure of one atmosphere. The interferometer was set to scan one FSR in 200 sec, and the signal was

processed through the ratemeter and recorded as a function of plate separation. The results are shown in Fig. 10. A comparison of Figs. 8 and 10 demonstrates the ability of the Fabry-Perot interferometer to reject the unwanted rotational Raman signal from CO_2 while at the same time detecting the N_2 scattering signal.

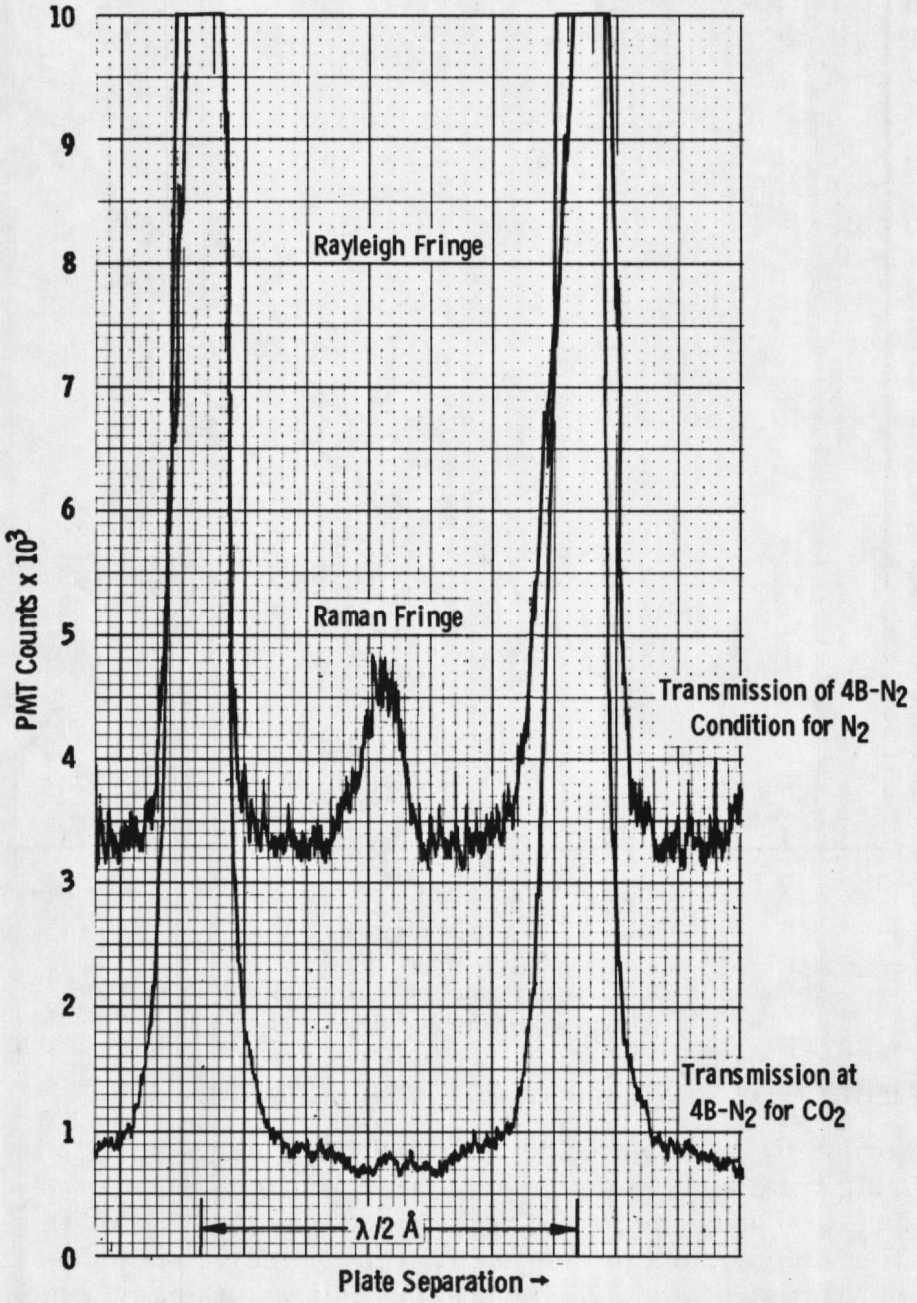

Figure 10. Pure rotational Raman spectrum for CO_2: transmitted pattern with the FPI set to pass only N_2 rotational Raman lines.

4.0 THEORETICAL PERFORMANCE CALCULATIONS

The preceding discussion, experimental results, and comparison of the Fabry-Perot count rates with previously acquired Raman data (Ref. 11) demonstrates the gain in system sensitivity which can be realized by using Fabry-Perot interferometry for Raman scattering of simple molecular gases. However, an increase in sensitivity, or detectivity, is a necessary but not sufficient condition for the consideration of use of the technique for flow diagnostics applications. It has been seen that the total transmitted intensity (I_T) is linearly dependent on gas density for room temperature. A pertinent feature, however, regarding studies of flow fields with values of T_R which vary significantly throughout the flow, is the variation of I_T with T_R. That is to say, is I_T dependent not only on gas density but also on T_R, and, if so, with what precision must T_R be known to yield a specified precision in number density. Additionally, for flow fields for which the vibrational temperature (T_v) exceeds T_R, the variation of the RRS intensities must be evaluated as a function of the degree of vibrational nonequilibrium. To quantitatively evaluate the magnitude of these effects, an analysis of the variation of the RRS intensities with T_R and T_v was performed; the following paragraphs outline these calculations and their results.

Since the primary application of this technique is for flow fields whose constituents are simple molecular species, such as N_2, O_2, H_2, HF, and CO_2, the molecule is assumed to be a rigid rotator with vibrational-rotational coupling manifested by a vibrational quantum (v)-dependent rotational constant (B_v). Further, the molecular species is assumed to be characterized by a singlet ground electronic state; although this is not the case for O_2, the neglect of its triplet fine structure is justified for the purposes of this calculation.

It is known that the Stokes (S-branch) and anti-Stokes (O-branch) RRS intensities (I_J^{+2} and I_J^{-2}, respectively) can be represented as (Ref. 12):

$$I_J^{+2} = (\lambda_o/\lambda_J^{+2})^4 \; b_{J+2}^J \times [n(v,J)/n_T] \;, \quad J \geq 0 \qquad (9)$$

and

$$I_J^{-2} = (\lambda_o/\lambda_J^{-2})^4 \; b_{J-2}^J \times [n(v,J)/n_T] \quad , \quad J \geq 2 \tag{10}$$

where $b_{J'}^J$ is the photon-molecule RRS strength factor for the $J \rightarrow J'$ transition, λ_o is the incident laser wavelength, λ_J^{+2} and λ_J^{-2} are the wavelengths of the S and O branches, respectively, and $n(v, J)/n_T$ is the fraction of molecules in vibrational level (v) and rotational level (J). All unimportant geometrical and fundamental constants have been neglected.

It is assumed that the rotational mode of motion is characterized by a Boltzmann distribution and, consequently, a rotational temperature (T_R). Further, the vibrational mode is also to be Boltzmann and characterized by T_V. Since all molecules of interest for this work are linear, two rotational degrees of freedom exist, and for all species, except CO_2, only one vibrational mode exists. For CO_2, the possibility of multiple T_V's has not been allowed, and further work is required to achieve realistic CO_2 results for cases of significant vibrational excitation. Obviously, the calculation of I_J^{+2} and I_J^{-2} using Eqs. (9) and (10) requires: (a) calculation of the S and O branch wavelengths, (b) calculation of the appropriate strength factors $b_{J'}^J$, and (c) determination on $n(v, J)/n_T$ for various values of T_R, T_V, and molecular constants.

For the model assumed, the rotational term value F(v, J) is

$$F(v,J) = B_v J(J + 1) \tag{11}$$

where higher order terms are neglected. It is easily seen that this neglect introduces an error in F(v, J) of less than approximately one part per thousand for values of $J \leq 10$ for N_2. It is well-known that

$$B_v = B_e - \alpha_e (v + 1/2) \tag{12}$$

Consequently, the wave number change $\Delta\omega(v, J)$ is given by

$$\Delta\omega(v,J) = \mp 4B_v(J + 3/2) \quad , \quad J \geq 0 \tag{13}$$

where the upper and lower signs are the O and S branches, respectively, and J is the lower level J value.

The RRS line strengths for the S and O branches are given by (Ref. 12):

$$b^J_{J+2} = (3/2)(J + 1)(J + 2)/[(2J + 1)(2J + 3)] \quad , \quad J \geq 0 \tag{14}$$

and

$$b^J_{J-2} = (3/2)\,J(J - 1)/[(2J - 1)(2J + 1)] \quad , \quad J \geq 2 \tag{15}$$

Obviously, b^J_{J-2} is zero for J = 0 and 1, and it is to be noted that, here, J is the initial level quantum number. Further, it is of interest to take note of the magnitude of the $b^J_{J\pm2}$ coefficients, and Table 1 lists these

Table 1. Rotational Raman Scattering Strength Factors $b^J_{J\pm2}$.

J	$b^{J,0}_{J+2,0}$	$b^{J,0}_{J-2,0}$
	J = 0,1,2,...	J = 2,3,4,...
0	1.000	0
1	0.6000	0
2	0.514285	0.2000
3	0.47619	0.25714
4	0.45454	0.28571
5	0.44056	0.30303
6	0.43077	0.31468
7	0.42353	0.32308
8	0.41796	0.32941
9	0.41353	0.33436
10	0.40994	0.33834
11	0.40696	0.34161
12	0.40444	0.34435
13	0.402298	0.34667
14	0.40044	0.34866
15	0.39883	0.35039
16	0.39740	0.35191
17	0.39614	0.35325
18	0.39501	0.35444
19	0.39400	0.35551
20	0.39308	0.35647
21	0.39225	0.35734
22	0.39149	0.35814
23	0.39079	0.35886
24	0.39016	0.35953
25	0.38757	0.36014
26	0.38902	0.36071
27	0.38852	0.36123
28	0.38805	0.36172
29	0.38761	0.36218
30	0.38720	0.36260
40	0.38420	0.36568
50	0.38239	0.36754
100	0.37872	0.37126

values for a range of J values. Their relative constancy for $J \gtrsim 3$ is to be noted. Finally, the limiting value of b^J_{J+2} as $J \to \infty$ is

$$\lim_{J\to\infty} b^J_{J+2} = (3/2)\left[\lim_{J\to\infty}\left(\frac{J+1}{2J+1}\right)\right]\left[\lim_{J\to\infty}\left(\frac{J+2}{2J+3}\right)\right]$$

$$= 3/8 = 0.3750 \tag{16}$$

where, since the $b^J_{J\pm2}$ sequences are convergent, the limit of a product is the product of the limits. An identical result follows for $\lim_{J\to\infty} b^J_{J-2}$.

The calculation of the number density distribution function $n(v, J)/n_T$ is somewhat more tedious. Since the rotational energy E(v, J) is given by

$$E(v,J) = hc \times F(v,J) \tag{17}$$

and vibration-rotation coupling is included,

$$n(v,J)/n_T = [n(v)/n_T] \times [n(v|J)/n_T] \tag{18}$$

where $n(v)/n_T$ is the fraction of molecules in vibrational level (v) and $n(v|J)/n_T$ is the fraction of molecules in level (J) given that the vibrational level is v. Obviously, $n(v|J)/n_T$ is a conditional probability function. If G(v) is the vibrational term value for level (v) for the Morse oscillator,

$$G(v) = \omega_e(v + 1/2) - \omega_e x_e(v + 1/2)^2 \tag{19}$$

where ω_e and $\omega_e x_e$ are the vibrational frequency and anharmonicity factors, respectively, in wave number units. The vibrational energy E(v) is

$$E(v) = h \times c \times G(v) \tag{20}$$

therefore,

$$n(v)/n_T = \exp[-hc\,G(v)/kT_v]/Q_v \tag{21}$$

where Q_v is the vibrational partition function. The task remaining is the calculation of $n(v|J)/n_T$; for a heteronuclear specie,

$$n(v|J)/n_T = (2J + 1)\exp[-hc\,B_v J(J + 1)/kT_R]/Q_R \tag{22}$$

where Q_R is the rotational partition function. For a homonuclear species of nuclear spin I, nuclear atomic number A, and symmetric electronic eigenfunction with respect to interchange of nuclei for even A molecules

$$n(v/J)n_T = \frac{I - 1}{2I - 1} \times \frac{(2J + 1) \exp [- hc F(v,J)/kT_R]}{Q_E} \tag{23}$$

for

$$J = 0, 2, 4, \ldots$$

and

$$n(v'J)/n_T = \frac{I}{2I + 1} \times \frac{(2J + 1) \exp [- hc F(v,J)/kT_R]}{Q_o} \tag{24}$$

where

$$Q_E = \sum_{J=0,2,4 \ldots}^{\infty} (2J + 1) \exp [- hc F(v,J)/kT_R]$$

and

$$Q_o = \sum_{J=1,3,5, \ldots}^{\infty} (2J + 1) \exp [- hc F(v,J)/kT_R]$$

For odd A species, the spin multiplicative factors (I + 1)(2I + 1) and I/(2I + 1) are reversed in Eqs. (23) and (24) for even and odd J.

A computer program was written, which performs the calculation of Eqs. (9) and (10) using the relations just presented. The results of this calculation only for N_2 will be discussed in this report. The computed parameters include $I_J^{+2,-2}$, $I_T^{-2,-2} = \Sigma_J I_J^{+2,-2}$, the ratio I_T^{-2}/I_T^{-2}, and Q_E and Q_O for each vibrational level v. The intensity functions are, of course, weighted by the fraction $n(v)/n_T$, which was computed according to the equation,

$$n(v)/n_T = [1 - \exp(-u)] \exp [-uv(1 - x_e v)(1 + x_e)]/1 + [2x_e v_{exp}(-2u)][1 - \exp(-u)]^{-2} \tag{25}$$

where

$$u = hc(\omega_e - \omega_e x_e)/k$$

Figure 11 shows the variation of $Q_{E,O}$ for N_2 with T_R; the vibrational levels v = 0 and 2 are shown explicitly to indicate the difference to be

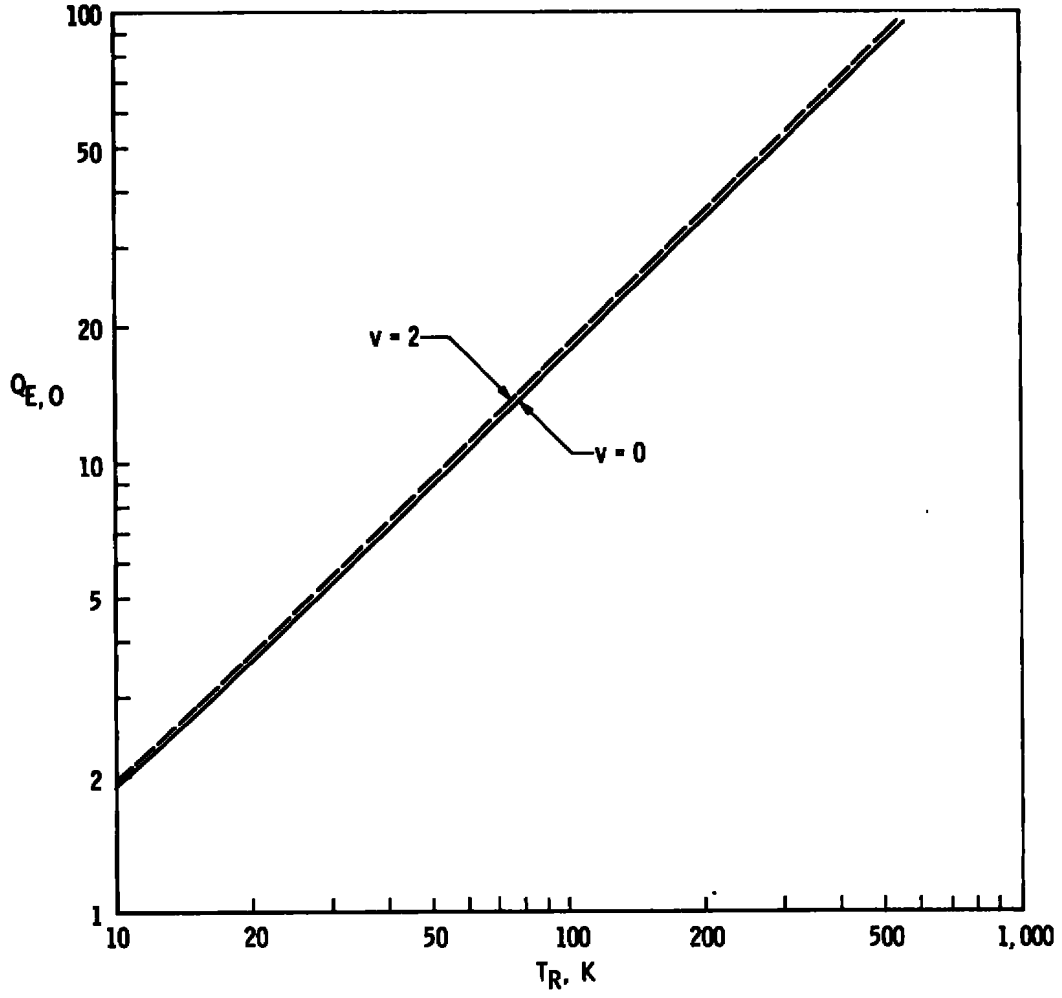

Figure 11. Variation of rotational partition functions Q_E and Q_O with rotational temperature T_R of N_2.

expected in $Q_{E,O}$ as a result of vibration-rotation coupling. For an argon-ion laser line of wavelength 514.52 nm, the variations with T_R of the S and O branch total intensities I_T^{+2} and I_T^{-2}, respectively, were calculated, and Fig. 12 shows the results. T_V is assumed here to be sufficiently low to preclude significant vibrational excitation. For N_2, this condition is

satisfied for $T_v \lesssim 1,000$ K. Since I_T, the sum of I_T^{+2} and I_T^{-2}, is the parameter determined by operating the FPI at the 4B resonance condition, the variation of I_T with T_R is also shown in this figure. Since I_T^{+2}, I_T^{-2}, and I_T are all linearly dependent on the density n_T, the constancy of I_T with T_R demonstrates that n_T can be determined uniquely using the FPI without any correction for T_R. The ratio I_T^{-2}/I_T^{+2} is shown in Fig. 13 as a function of T_R, and the ability to determine T_R using this ratio is obvious. Clearly, the use of a spectral blocking filter, or its equivalent, will be required to pass only I_T^{+2} in the first instance and then upon its removal to pass $I_T^{+2} + I_T^{-2}$. The variation of I_T and I_T^{-2}/I_T^{+2} with T_R is also shown in Fig. 14 for which the low temperature limit is clearly seen. The deviation of I_T from its constant value becomes significant for $T_R \sim 10\theta_R$ where θ_R is the characteristic temperature of the species and is given by

$$\theta_R = hc\, B_v/k$$

which for N_2 is approximately 2.88 K. The limiting values of $I_T^{+2,-2}$ as $T_R \to 0$ are of interest. For heteronuclear molecules, the population number density collapses to the J = 0 level as $T_R \to 0$ and

$$\lim_{T_R \to 0} I_T^{-2} = 1$$

$$\lim_{T_R \to 0} I_T^{-2} = 0$$

For homonuclear molecules, a different situation arises. For the assumed model for even A species, one can easily show that

$$\lim_{T_R \to 0} I_T^{+2} = (1.6\,I - 1)/(2I + 1)$$

and, as before,

$$\lim_{T_R \to 0} I_T^{-2} = 0$$

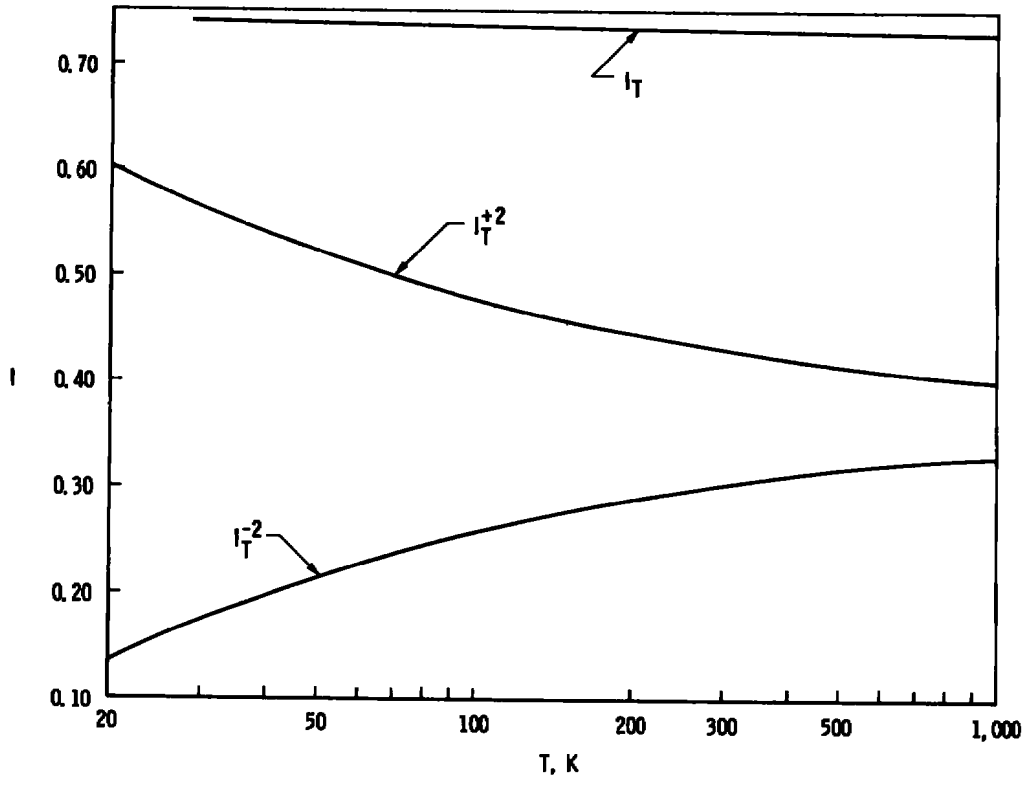

Figure 12. Temperature variation of rotational Raman intensity parameters for N_2.

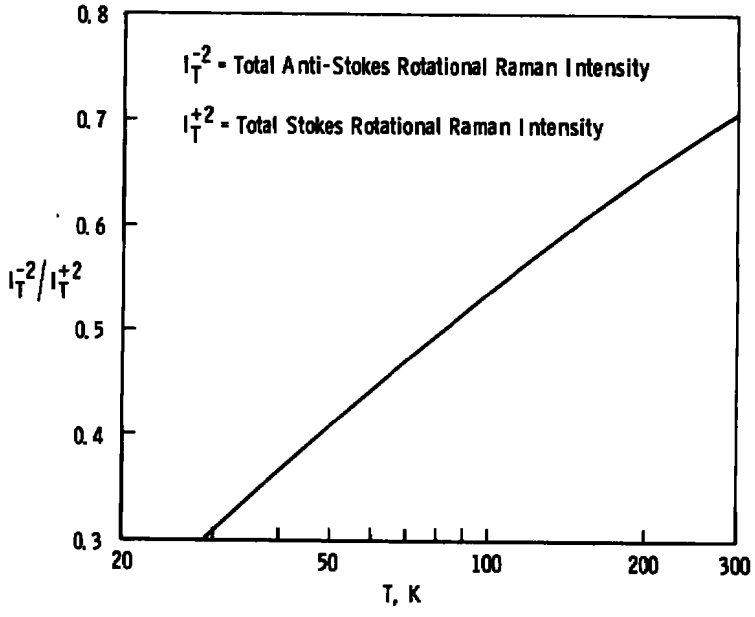

Figure 13. Temperature variation of rotational Raman anti-Stokes-to-Stokes ratio for N_2.

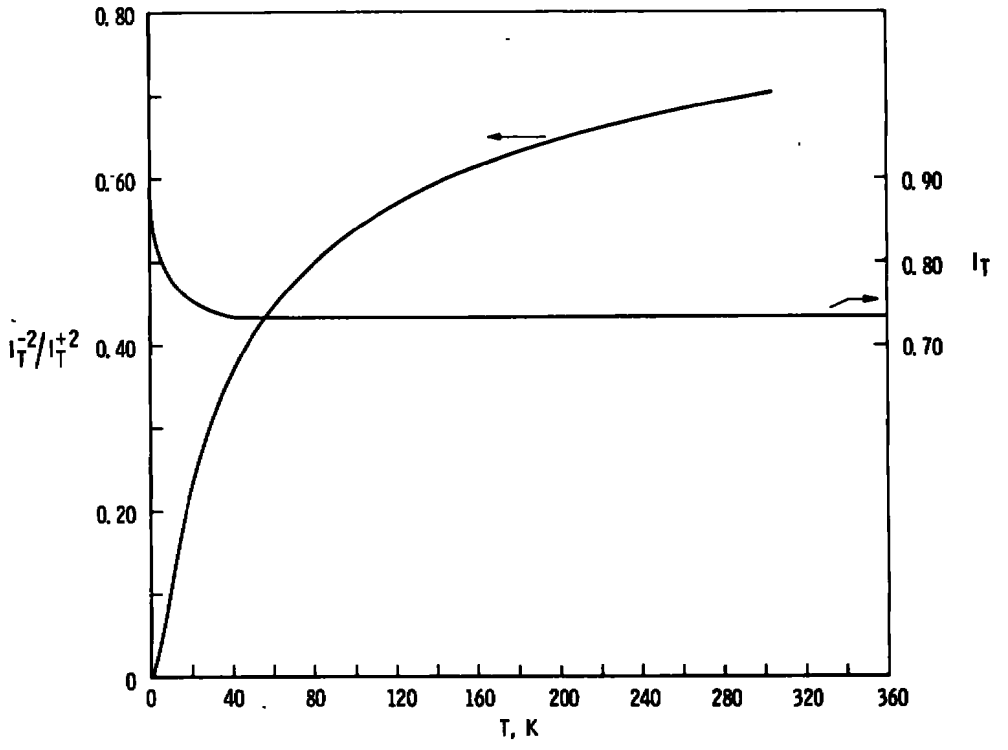

Figure 14. Temperature variation of rotational Raman intensity parameters for N_2.

For odd A species,

$$\lim_{T_R \to 0} I_T^{+2} = (1.6I + 0.6)/(2I + 1)$$

and again $I_T^{-2} \to 0$. Table 2 exhibits these limiting values for the range of nuclear spin of 0 to 2.

Finally, the effects of variation of T_v on the results for the RRS intensity functions were investigated for the T_v range from 300 to 3,000 K, and Fig. 15 shows the variation of n_v/n_T of N_2 with T_v. For $T_v \sim 1{,}000$ K, it is seen that the contribution from vibrational levels $v \geq 1$ is on the order of 3 percent or less. It was found that the calculated values of the ratio I_T^{-2}/I_T^{+2} for the individual vibrational levels v = 0, 1, and 2 differed by no more than 2 percent; i.e., I_T^{-2}/I_T^{+2} is essentially independent of the vibrational level for which RRS occurs. The variation of I_T^{+2} with T_v is shown in Fig. 16 for the v = 0 level species for T_R = 10, 20, and 100 K. The

Table 2. Spin Dependence of I_T^{+2} for $T_R = 0$.

Type \ I	0	1/2	1	3/2	2
Even A	1.000	0.9000	0.8667	0.8500	0.8400
Odd A	---	0.7000	0.7333	0.7500	0.7600

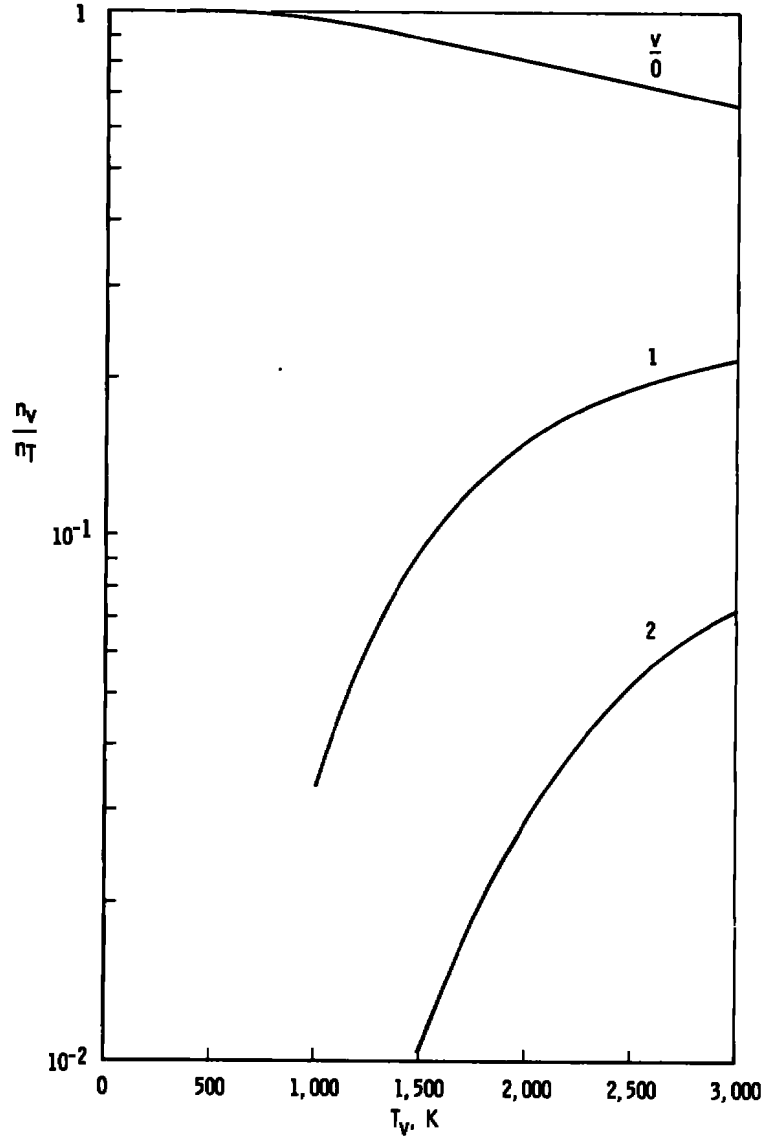

Figure 15. Variation of $n(v)/n_T$ of N_2 with T_v.

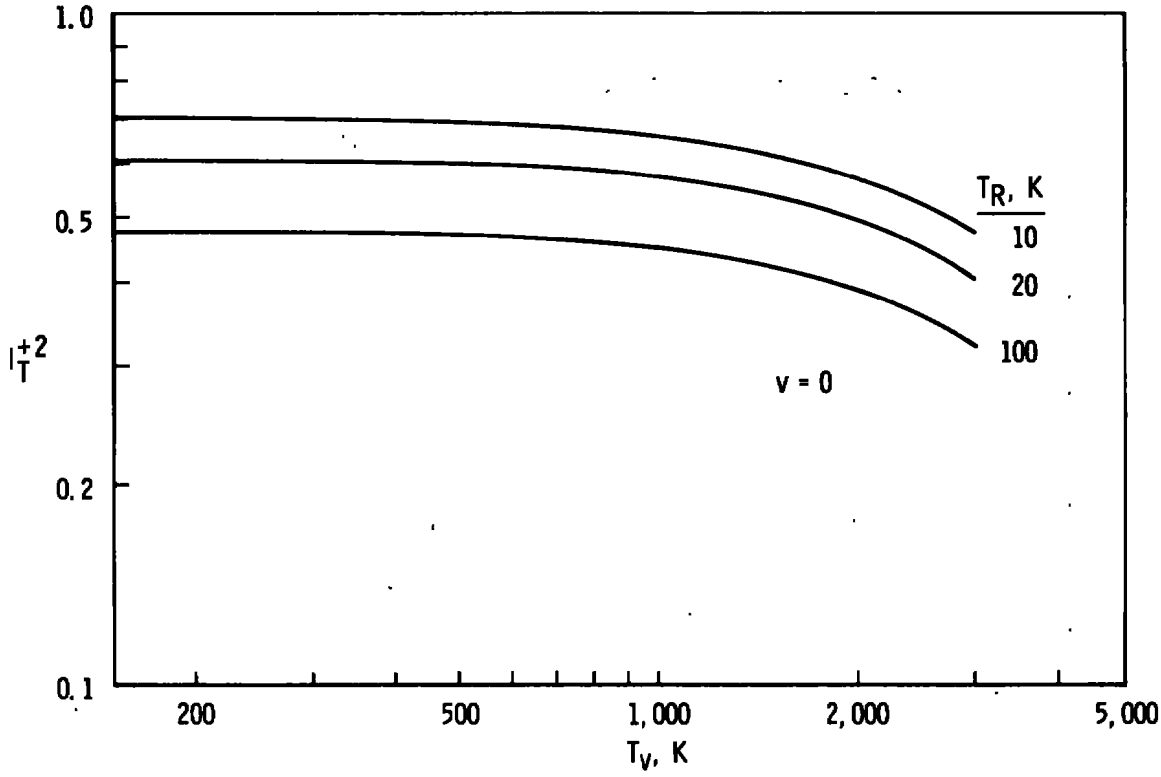

Figure 16. Variation of the total Stokes RRS intensity I_T^{+2} with vibrational temperature T_v for N_2.

decrease in I_T^{+2} with T_V is clearly a result of the depletion of v = 0 molecules with increasing T_V. In Fig. 17 is shown the variation with T_V of I_T for v = 0 at T_R = 10, 20, and 100 K. The decrease in I_T with T_V is seen to be smaller than that of I_T^{+2} with T_V. Also shown in Fig. 17 is the sum of intensities I_T^{+2} for the vibrational levels v = 0, 1, and 2 for T_R = 20 and 100 K. It is seen from Fig. 17 that significant variations in the value of I_T for v = 0 occur as T_V increases above approximately 1,000 K. Consequently, the use of the 4B resonance condition of the FPI for RRS measurements of N_2 gas number density requires a correction for the vibrational temperature if $T_V \gtrsim 1,000$ K. Of course, separate measurements of I_T for v = 0 and either v = 1 or v = 2, or both, each at their respective 4B plate separations provides an experimental measurement of T_V, which then can be used for correction of the I_T data.

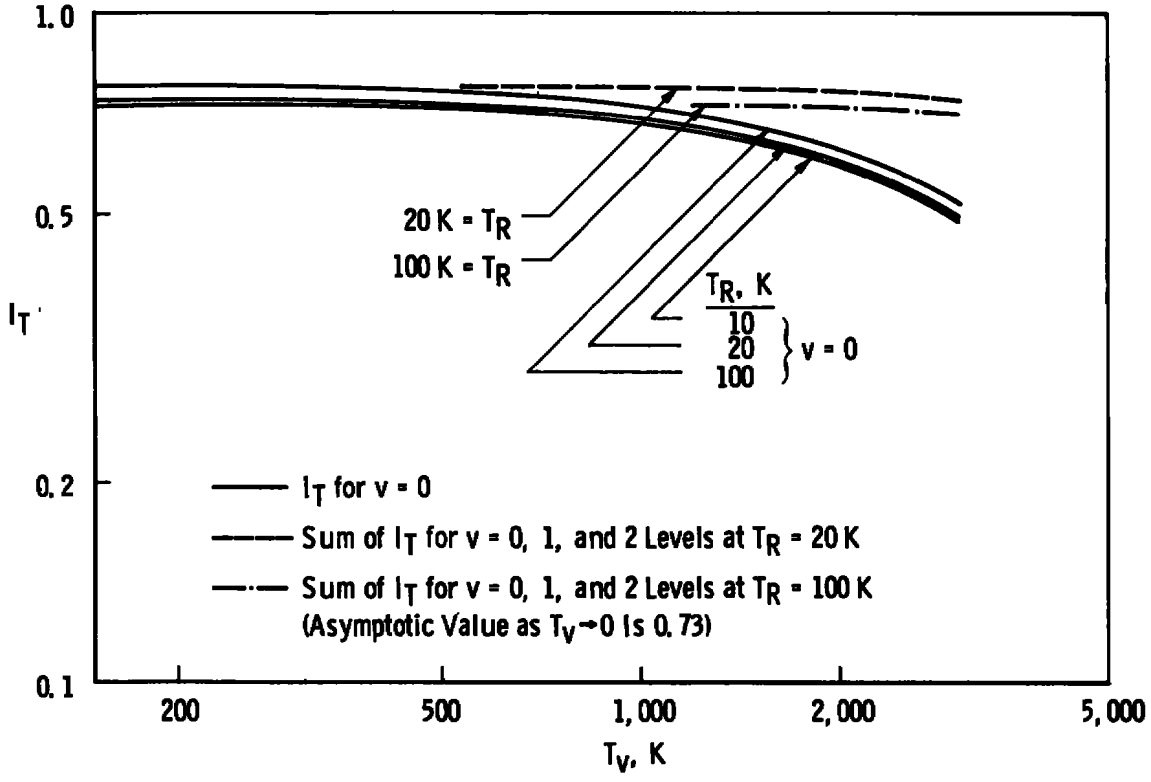

Figure 17. Variation of RRS intensity I_T with vibrational temperature T_v.

5.0 DISCUSSION AND CONCLUSIONS

The experimental FPI results demonstrate the advantages to be gained in sensitivity of the Raman scattering measurement of gas density. A comparison of the peak amplitudes for the Rayleigh scattered intensity and the Raman scattered intensity shows this conclusion quite clearly if one recalls that the ratio of Rayleigh and rotational Raman scattering cross sections is on the order of 1,000. The pressure variation of the Raman signal transmitted by the FPI for N_2 at room temperature shows the linearity of the FPI Raman signal with gas density, and thereby, its potential use for flow field diagnostics. Additionally, the rejection of the CO_2 signal by the Fabry-Perot when used with plate separations appropriate for the 4B resonance case of N_2 demonstrates the potential use of the technique for gas mixtures of CO_2 and N_2.

The calculated variation of the RRS intensity function with rotational temperature, the sum of the intensities S and O branches, shows for N_2

the potential absence of any correction to the measured gas density for T_R. Consequently, there is a one-to-one correspondence between I_T and N_2 number density so long as $T_V \lesssim 1,000$ K. For higher values of T_V, the vibrational temperature must be known or measured, the latter of which can be performed using the spectrally resolved contributions of I_T from the individual vibrational levels.

The enhancement of spectrometric speed of the Fabry-Perot system, its apparent ability to provide measurements of gas number density, rotational and vibrational temperatures, and the compactness of the instrument all provide incentive for continuation of the investigation of the technique. Current research efforts in this area include the investigation of its application to studies of other single gaseous species, binary and multiple specie mixtures, and flow field studies. The interfacing of the device with an image intensifier/vidicon is in progress, and this step will yield the full advantages of multiplexing by observing all the ring patterns simultaneously. Additionally, the use of a spectral blocking filter with the FPI for T_R measurements is planned.

REFERENCES

1. Lewis, J. W. L. and Williams, W. D. "Measurements of Temperature and Number Density in Hypersonic Flow Fields Using Laser Raman Spectroscopy." AIAA Paper No. 75-175, Presented at the AIAA 13th Aerospace Sciences Meeting, Pasadena, California, January 20 to 22, 1975.

2. Lewis, J. W. L., Williams, W. D., and Powell, H. M. "Laser Diagnostics of a Condensing Binary Mixture Expansion Flow Field." Rarefield Gas Dynamics, edited by M. Becker and M. Fiebig, 9th Symposium, Vol. II, pp. F7.1-F7.8, 1974, DFVLR Press, Porz-Wahn, Germany.

3. Barrett, J. J. and Myers, S. A. "A New Interferometric Method for Studying Periodic Spectra Using a Fabry-Perot Interferometer." Journal of the Optical Society of America, Vol. 61, No. 9, 1971, pp. 1246-1251.

4. Barrett, J. J. "The Use of a Fabry-Perot Interferometer for Studying Rotational Raman Spectra of Gases." Laser Raman Gas Diagnostics, Plenum Press, New York, 1974, p. 63.

5. Barrett, J. J. and Harvey, A. B. "Vibrational and Rotational-Translational Temperatures in N_2 by Interferometric Measurements of the Pure Rotational Raman Effect." Journal of the Optical Society of America, Vol. 65, No. 4, 1975.

6. Born, M. and Wolf, E. Principles of Optics. Pergamon Press, London, 1970.

7. Herzberg, G. Spectra of Diatomic Molecules. D. Van Nostrand Company, Inc., New York, 1950.

8. Smith, W. H. "A New Method for the Detection of Raman Scattering from Atmospheric Pollutants." Opto-Electronics, Vol. 4, 1972, pp. 161-7.

9. Hargis, P. J. and Hill, R. A. "Fabry-Perot Interferograms of Periodic Spectra of Molecules with Large Rotational Constants." Journal of the Optical Society of America, Vol. 65, No. 2, 1975, pp. 219,220.

10. Schwiesow, R. L. "Optimum Illumination Geometry for Laser Raman Spectroscopy." Journal of the Optical Society of America, Vol. 59, No. 10, October 1969, pp. 1285-1287.

11. Williams, W. D. and Lewis, J. W. L. "Rotational Temperature and Number Density Measurements of N_2, O_2, CO, and CO_2 in a Hypersonic Flow Field Using Laser-Raman Spectroscopy." AEDC-TR-75-37 (ADA012877), July 1975.

12. Sushchinskii, M. M. Raman Spectra of Molecules and Crystals. Israel Program for Scientific Translations, New York, 1972.

NOMENCLATURE

A	Absorptance, atomic number
B	Rotational constant
$b_J^{J'}$	Scattering strength factor
c	Speed of light
d	Plate separation distance

$E(v, J)$	Energy of rotation-vibration level (v, J)
FSR	Free spectral range
$F(v, J)$	Term value for energy E(v, J)
FPI	Fabry-Perot interferometry (or interferometer)
h	Planck's constant
I	Nuclear spin
$I_J^{+2,-2}$	Intensity of rotational Raman scattering for level J for S(+2) and O(-2) branches
$I_T^{+2,-2}$	Intensity of the sum of all $I_J^{+2,-2}$ for S and O branches
I_T	Total intensity, sum of I_T^{+2} and I_T^{-2}
I_t	Transmitted intensity
I_o	Incident intensity
J	Rotational quantum number
m	Order of interference
n, n_T	Gas number density
$n(v, J)/n_T$	Fraction of molecules in level v, J
$n(v\|J)/n_T$	Fraction of molecules in rotational level J given that the vibrational level is v
$n(v)/n_T$	Fraction of molecules in vibrational level v
P_o	Gas pressure
Q	Partition function
Q_E	Even J partition function
Q_O	Odd J partition function
Q_v	Vibrational partition function
R	Reflectance
RRS	Rotational Raman scattering
T	Transmittance
T_R	Rotational temperature
T_v	Vibrational temperature

T_o	Gas temperature
β	Solid angle
δ	Phase change parameter
λ	Wavelength
μ	Index of refraction
Φ	Phase change parameter
ϕ'	Angle of refraction
Ω	Collective solid angle
ω	Angular frequency in wavenumber units
$\Delta\omega$	Angular frequency interval, free spectral range
ω_J	Frequencies of the pure rotational Raman lines
ω_o	Frequency of the laser exciting source

Note: All units are metric unless otherwise specified.